MRI Isotropic Resolution Reconstruction from two Orthogonal Scans

José G. Tamez-Peña [*a], Saara Totterman [**b] and Kevin J. Parker [***a]

[a]Department of Electrical and Computer Engineering, University of Rochester;
[b]Department of Radiology, Medical Center, University of Rochester

ABSTRACT

An algorithm for the reconstructions of ISO-resolution volumetric MR data sets from two standard orthogonal MR scans having anisotropic resolution has been developed. The reconstruction algorithm starts by registering a pair of orthogonal volumetric MR data sets. The registration is done by maximizing the correlation between the gradient magnitude using a simple translation-rotation model in a multi-resolution approach. Then algorithm assumes that the individual voxels on the MR data are an average of the magnetic resonance properties of an elongated imaging volume. Then, the process is modeled as the projection of MR properties into a single sensor. This model allows the derivation of a set of linear equations that can be used to recover the MR properties of every single voxel in the ISO-resolution volume given only two orthogonal MR scans. Projections on convex sets (POCS) was used to solve the set of linear equations. Experimental results show the advantage of having a ISO-resolution reconstructions for the visualization and analysis of small and thin muscular structures.

Keywords: MRI, ISO-resolution reconstruction, Filtered back-projection, POCS

1. INTRODUCTION

For many clinical applications standard Magnetic Resonance Imaging (MRI) provides excellent images for a trained human eye. This technology can generate images with high contrast among various soft tissues and organs. As a result, MRI has become the modality of choice in many diagnostic studies of the head, spine, and joints.[1] But for an automatic joint-motion analysis an autonomous system has to be able to segment several small and similar structures. To improve the structure to structure contrast for improved brain segmentation several algorithms have been developed which fuse two or more same plane brain MR imaging data sets.[2,3] Although these multi-parameter data sets improve the tissue contrast, they however do not improve the resolution. Based on our experience the segmentation of musculoskeletal structures on MR images cannot be accomplished unless the resolution is improved.[4,5] The existing in-plane resolution with 300-400 micron pixel size is sufficient; however, the slice thickness of 1 mm or higher is too large. Decrease in signal to noise ratio and limitations of gradient strength have hindered the use of thinner slices. However if two orthogonal data sets are registered and fused that will result in a 3-dimensional data set where voxel size and the thickness of the reformatted slices will correspond to the in-plane resolution of the original images. Therefore we developed an algorithm which registers and fuses two orthogonal 3D musculoskeletal imaging data sets and creates 3D isotropic volume data set. Goshtasby[6] proposed the fusion of long axis and short axis images of the heart to enhance the image resolution. Here we propose a similar approach but with general applications on MR images. In this paper we validate registration and fusion of the algorithm by comparing the resolution in the fused data set to the original data set.

2. ORTHOGONAL IMAGE FUSION

The low inter-slice resolution inherent in MRI imaging is overcome by using two volumetric data sets. The scanning directions of the data sets has to be orthogonal to each other, and then the data can be fused together in a single high-resolution image. Figure 1 shows different MRI slices of two volumes of the shoulder taken at two different orthogonal scanning planes. Although the fusion of the two volumes seems to be trivial, there are two issues that have to be taken into account 1) the registration among volumes scanned at different time and 2) the overlapping of sampling voxel volumes.

[*]pena@ece.rochester.edu;phone 716 275-0033; http://www.ece.rochester.edu/~ pena; Dept. of Elec. and Comp. Eng. University of Rochester, Rochester, NY, USA 14627; [**] tot@rad.rochester.edu; University of Rochester, Medical Center; Rochester, NY, USA 14620; [***] parker@ece.rochester.edu; Dept. of Elec. and Comp. Eng. University of Rochester; Rochester, NY, USA, 14627

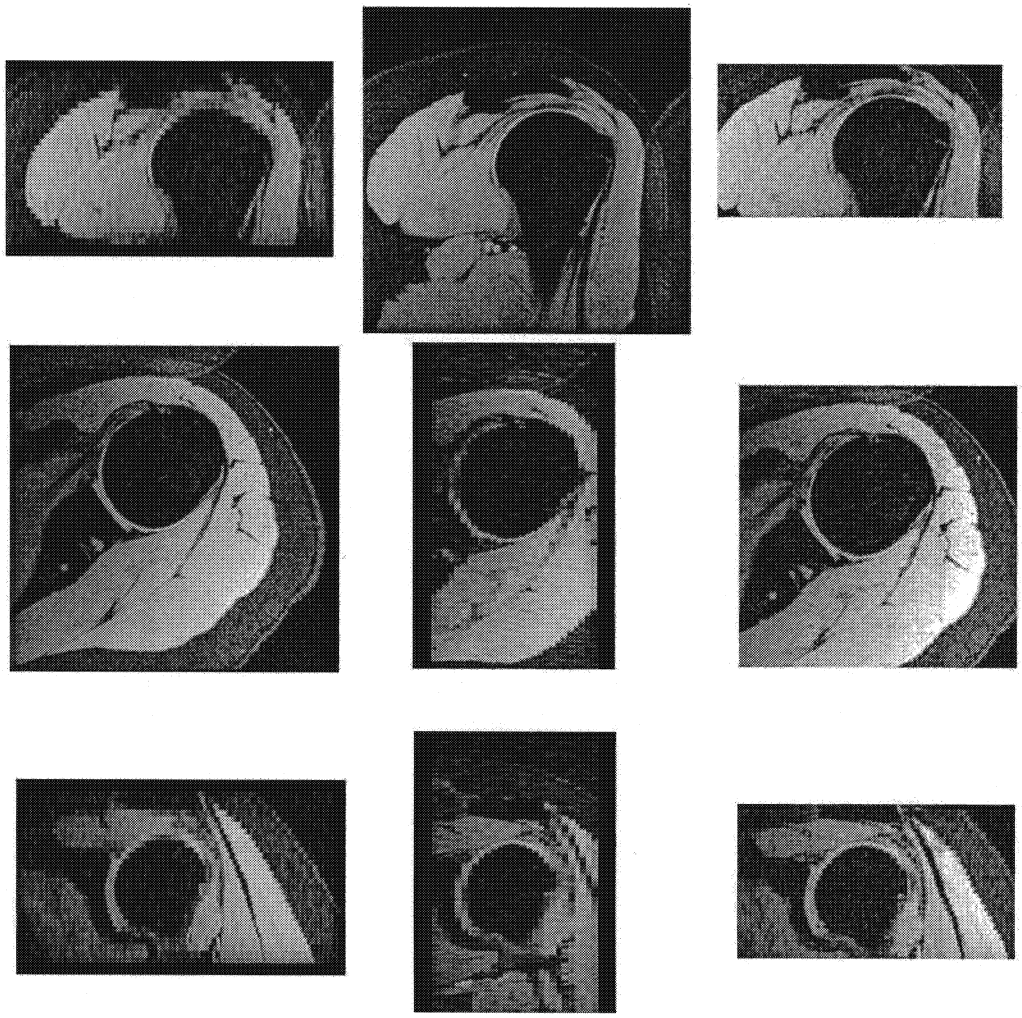

Figure 1. (a) axial, (b) sagittal, (c) coronal views of the original MRI sagittal scan (left images) and axial scan (central images) and the fused image (right images) of a human shoulder.

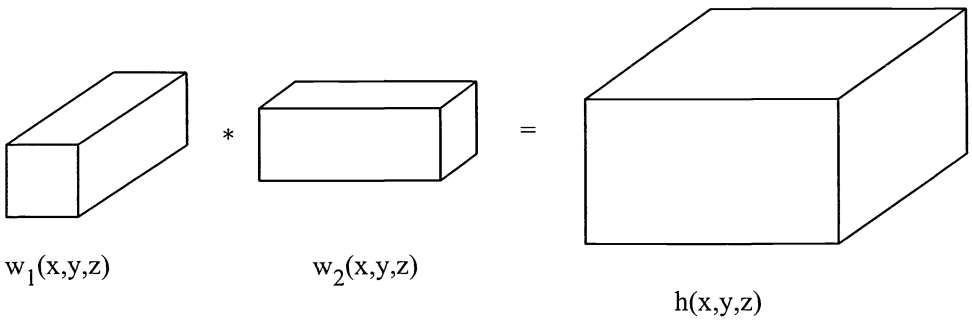

Figure 2. Supporting region of the blurring function.

2.1. Image Registration

Remember that the goal is to create a high resolution 3D image from the fusion of the two data sets. Therefore, the registration of both volumes has to be as accurate as the in-plane resolution. A lot of research has been done in the area of medical image registration

[7–10] which is designed to register misaligned data set. Although these techniques can be used to register orthogonal data sets, most of them are very complex. In this research it is proposed a very simple technique developed to register two very similar orthogonal MRI images. This registration is done by assuming a simple translation-rotation model; thus, a fair model for small and involuntary human motion between scans. We developed an unsupervised registration algorithm that finds the point (x, y, z) where the correlation between the two data sets is maximum which, by Schwartz inequality we know that is the point where they match. Assuming a translation model, and given two functions $u(x, y, z)$ and $v(x, y, z)$ the correlation is given by:

$$r(x,y,z) = u(x,y,z) * v(x,y,z) = \int\int\int u(\alpha,\beta,\gamma)v(x+\alpha, y+\beta, z+\gamma)d\alpha d\beta d\gamma. \quad (1)$$

If $u(x, y, z)$ is just a displaced version of $v(x, y, z)$, $u(x, y, z) = v(x + \Delta x, y + \Delta y, z + \Delta z)$, then the maximum is at $(-\Delta x, -\Delta y, -\Delta z)$, the displacement between both functions. For MRI we have to remember that every voxel in the magnetic resonance image is observing the average magnetization of an ensemble of protons at a small volume. We can model this as the correlation of the continuous image by a small 3D window. Let us call $g_1(x, y, z)$ and $g_2(x, y, z)$ the sampled volumes at two orthogonal directions and given by:

$$g_1(x,y,z) = f(x,y,z) * w_1(x,y,z) * \Pi(x,y,z) \quad (2)$$
$$g_2(x,y,z) = f(x+\Delta x, y+\Delta y, z+\Delta z) * w_2(x,y,z) * Pi(x,y,z), \quad (3)$$

where $w_1(x, y, z)$ and $w_2(x, y, z)$ are the 3D windows for the two orthogonal scanning directions, $(\Delta x, \Delta y \Delta z)$ is a small displacement, and $\Pi(x, y, z)$ is the sampling function. Therefore, the correlation of the two sampled volumes is

$$\begin{aligned} r(x,y,z) &= g_1(x,y,z) \cdot g_2(x,y,z) \quad (4)\\ &= f(x+\Delta x, y+\Delta y, z+\Delta z) * f(x,y,z) * w_1(x,y,z) * w_2(x,y,z) * \Pi(x,y,z). \end{aligned}$$

This is just a blurred version of the original correlation, the exact location of the maxima is shaped by the blurring function $h(x, y, z) = w_1(x, y, z) * w_2(x, y, z)$. That is, the correlation is distorted by the function of $h(x, y, z)$. Figure 2 shows an idealized window function for $w_1(x, y, z)$ and $w_2(x, y, z)$ and its corresponding supporting region of the blurring function, $h(x, y, z)$. Finding the displacement using the above procedure works fine for noise-free data; but noise makes this search more difficult. Let $g_1(x, y, z) = (f(x, y, z) + n_1(x, y, z)) * w_1(x, y, z)$ and $g_2(x, y, z) = (f(x + \Delta x, y + \Delta y, z + \Delta z) + n_2(x, y, z)) * w_2(x, y, z)$ be the corresponding noisy volumes, where $n_1(x, y, z)$ and $n(x, y, z)$ are two uncorrelated noise sources. Thus, the correlation of g_1 and g_2 is given by

$$r(x,y,z) = g_1(x,y,z) * g_2(x,y,z)$$

$$
\begin{aligned}
&= [f(x+\Delta x, y+\Delta y, z+\Delta z) * f(x,y,z) + \\
&\quad f(x+\Delta x, y+\Delta y, z+\Delta z) * n_1(x,y,z) + \\
&\quad f(x,y,z) * n_2(x,y,z)] * h(x,y,z) * \Pi(x,y,z),
\end{aligned} \tag{5}
$$

and the maximum is no longer guaranteed to be given by the displacement, especially for functions with smooth autocorrelation functions like standard MRI. The smooth autocorrelation functions makes the error bound to be function of the noise power. Autocorrelation functions whose shapes are closer to a Dirac delta function $\delta(x,y,z)$, are less sensitive to noise. The former is the reason that many registration algorithms work with edges.[8] The autocorrelation function of the gradient magnitude of standard MRI is closer to a Dirac delta function. Therefore, the registration of the gradient is less sensitive to noise. Figure 3 shows a 1D example of the effect of the derivative on the autocorrelation function of a band-limited signal. For this example a smooth derivative operator was used to reduce the noise level. Therefore, our automatic registration was based on finding the maximum on the correlation among the magnitude gradient of the two magnetic resonance images:

$$
(\Delta x, \Delta y, \Delta z) = \mathrm{Arg} \max_{(\Delta x, \Delta y, \Delta z)} \int\int\int ||\nabla g_1(\alpha,\beta,\gamma)||||\nabla g_2(\Delta x+\alpha, \Delta y+\beta, \Delta z+\gamma)|| d\alpha d\beta d\gamma, \tag{6}
$$

where in sampled images the gradient ∇ can be approximated by finite differences.

$$
||\nabla g(x,y,z)|| = \sqrt{d_x(x,y,z)^2 + d_y(x,y,z)^2 + d_z(x,y,z)^2}, \tag{7}
$$

where

$$
d_x(x,y,z) = \frac{l(x,y,z) * g(x+\delta x, y, z) - l(x,y,z) * g(x-\delta x, y, z)}{2\delta x}, \tag{8}
$$

$$
d_y(x,y,z) = \frac{l(x,y,z) * g(x, y+\delta y, z) - l(x,y,z) * g(x, y-\delta y, z)}{2\delta y}, \tag{9}
$$

$$
d_z(x,y,z) = \frac{l(x,y,z) * g(x, y, z+\delta z) - l(x,y,z) * g(x, y, z-\delta z)}{2\delta z}, \tag{10}
$$

where $\delta x, \delta y, \delta z$ are the sampling rates, and $l(x,y,z)$ is a low pass filter used to remove noise from the images and to compensate the differences between in-slice sampling and inter-slice sampling. The maximization of Equation 6 can be done using any standard maximization technique. We chose to use a simple hill-climbing technique, due to the fact that we are dealing with small displacements. The hill-climbing technique evaluates the correlation at the six orthogonal directions: up, down, left, right, front and back. The direction that has the biggest evaluation was chosen as the next position. This simple technique works well for the registration of two orthogonal data sets, as the one expected for involuntary motion during scans. To avoid being trapped in local maxima and to speed up the process, we used a multi-resolution approach. This multi-resolution approach consisted in selecting the hill-climbing step as half the size of the previous step. Five different resolutions were used. The coarser resolution selected was twice the in-plane resolution of the system, and the smallest size was just 25 percent of the in-plane resolution. Even though we used a very simple optimization approach the computation of the correlation of the whole data set can be time consuming; therefore, the registration of two images can take time. To speed up the correlation of the two data sets, we selected just a small subsample of the points with very high gradient, then those points were the ones used in the correlation process.

Some images suffer from a small rotation. In this case we extended the algorithm to search for the image rotation. The same hill-climbing technique was used to find the rotation between images; but instead of doing the search in a three-dimensional space, the algorithm has to look at a six-dimensional space. This search space included the three displacements and three rotations along each axis. At each step the rotation matrix was updated and used to compensate for the small rotation between images. Figure 4 shows the fusion of two orthogonal images of the knee data set, before and after registration.

2.2. Image Fusion

Once we registered the two images, we preceded to create an isotropic high resolution image from them. Due to the different shape between voxel sampling volumes ($w_2(x,y,z)$ and $w_1(x,y,z)$), one has to be careful when estimating every high resolution voxel value from the input data. Assume from our input pair that the first image has been

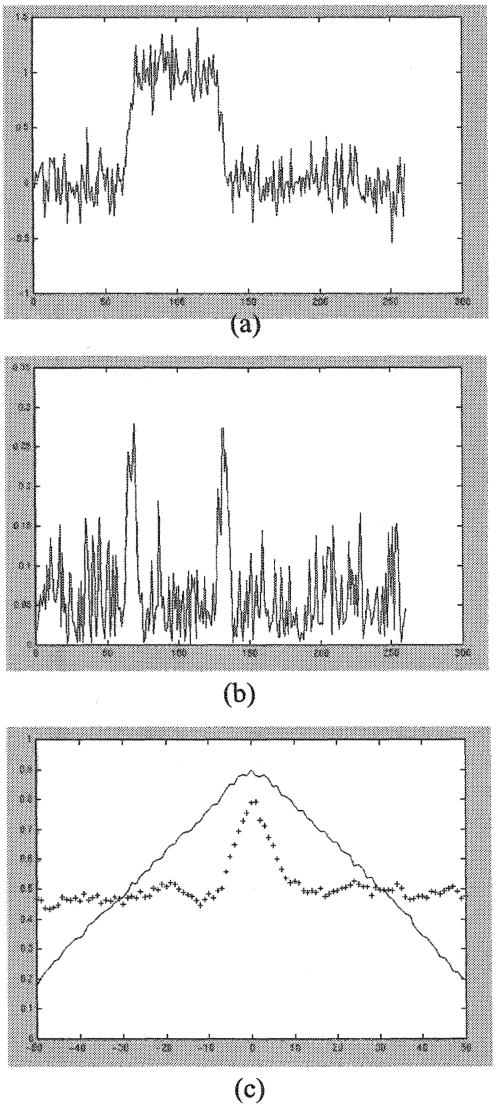

Figure 3. Correlation of a 1D function. (a) Original Signal f(x) (b) Smooth estimate of the derivative magnitude [g(x)=$|f(x) * [-1 \ -1 \ 0 \ 0 \ 0 \ 1 \ 1]|$. (c) Correlation: (-)f*f, (+) g*g.

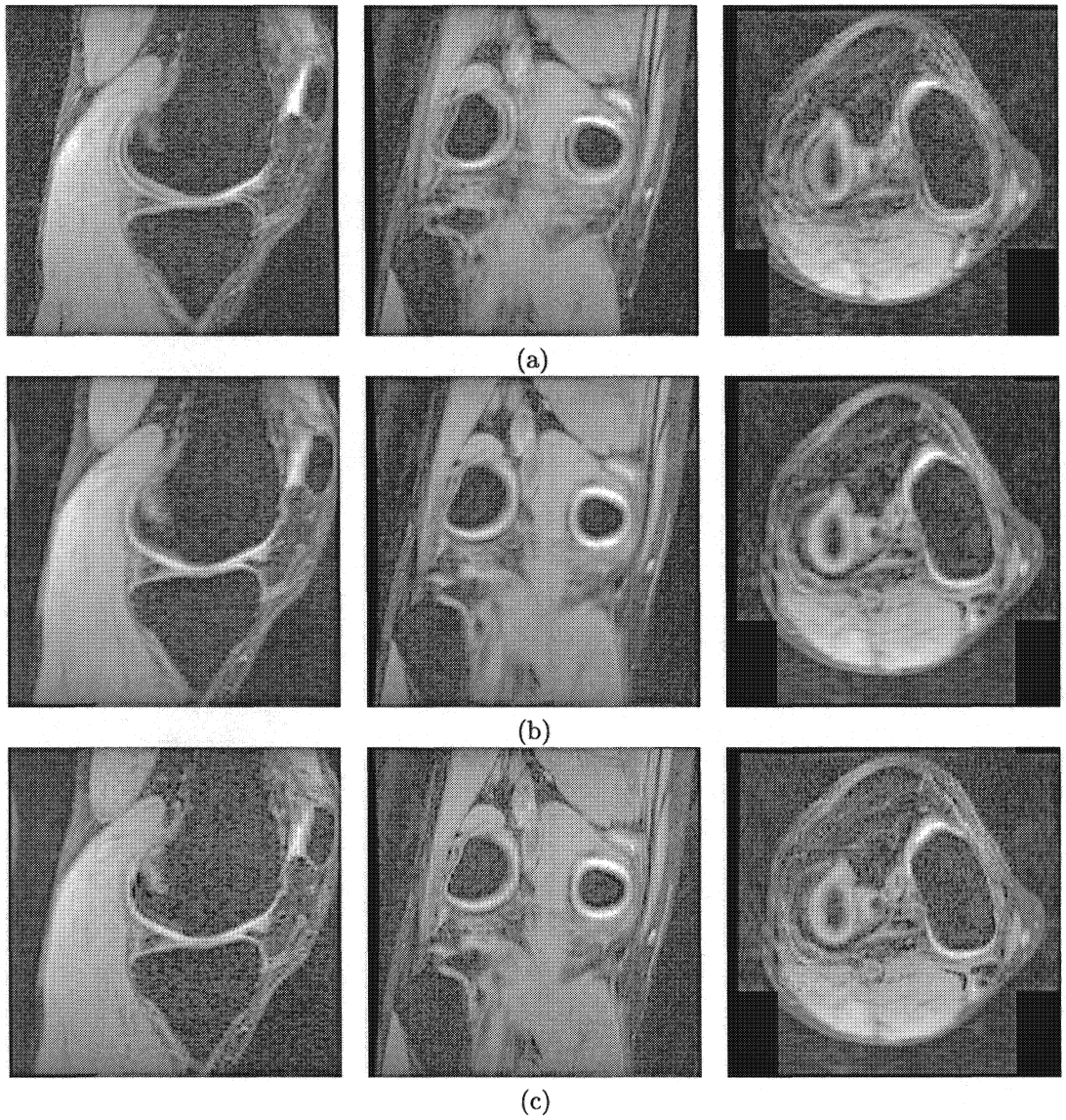

Figure 4. Image registration and fusion. (a) Axial, sagittal and coronal slices of simple fusion without registration, (b) simple fusion after registration, and (c) complete image fusion. The simple fusion is $g(x,y,z) = 0.5g_1(x,y,z) + 0.5g_2(x,y,z)$ and the complete fusion $g(x,y,z) = h_1(x,y,z) + h_2(x,y,z)$, where h_1, h_2 are the two functions that minimize the reconstruction error.

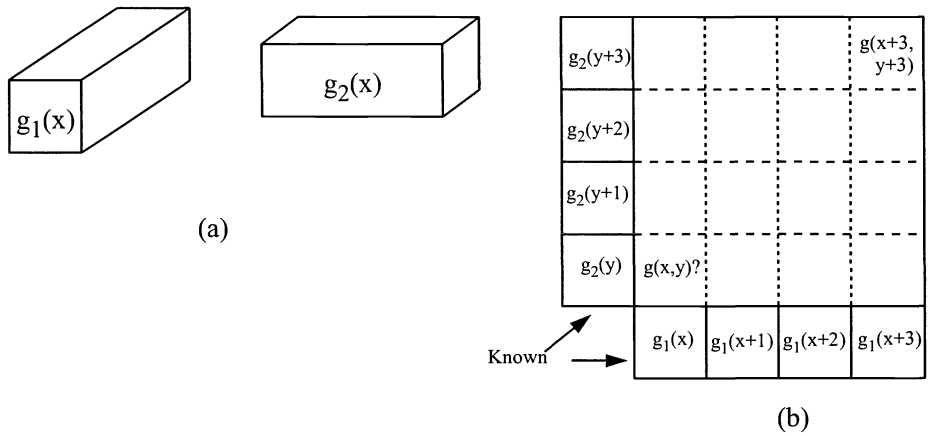

Figure 5. (a) 4 to 1 voxel shapes. (b) 2D representation of the known values in a 4x4 window for 4 to 1 aspect ratio voxels.

scanned in the x-direction and the other has been scanned in the y-direction. Therefore, there is high-resolution information at the z-direction in both images. Figure 5a shows the voxel shapes of the two input images, where the in-slice resolution is equal, and the inter-slice resolution is four times lower. Given this configuration, the problem of filling the high-resolution volume is a 2D problem. If we concentrate in a single 4x4-voxel window of the high resolution image, as seen in Figure 5b, then for every 16 high-resolution voxels there are only 8 known low-resolution voxels; therefore, this is an ill posed problem. To address this problem, assume that every high-resolution voxel is just a linear combination of the two low-resolution functions:

$$g(x,y,z) = h_1(x/s_d, y, z) + h_2(x, y/s_d, z), \tag{11}$$

where h_1, h_2 are two functions that are back projected in such a way that

$$g_1(x/s_d, y, z) = \sum_{\forall x \in w_1} g(x,y,z) \tag{12}$$

$$g_2(x, y/s_d, z) = \sum_{\forall y \in w_2} g(x,y,z). \tag{13}$$

This represents a linear system with the same number of knows as unknowns. The known values are the observed image voxels, while we estimate the values to back-project that match the observation. Noise and inhomogeneous sampling make the problem a little bit harder; but this linear system can efficiently be solved using projection on convex sets (POCS).[11] Although, in theory, all the components have to be orthogonally projected, it can be shown, that the following projecting scheme also works in this problem:

$$h_1^{k+1}(x/s_d, y, z) = h_1^k(x/s_d, y, z) - \alpha \frac{(n h_1^k(x/s_d, y, z) + \sum_{\forall x \in w_1} h_2^k(x, y/s_d, z) - g_1(x/s_d, y, z))n}{n^2+m} \tag{14}$$

$$h_2^{k+1}(x, y/s_d, z) = h_2^k(x, y/s_d, z) - \alpha \frac{(m h_2^k(x, y/s_d, z) + \sum_{\forall y \in w_2} h_1^k(x/s_d, y, z) - g_2(x, y/s_d, z))m}{n+m^2}, \tag{15}$$

where $0 < \alpha < 1$, $n = \sum_{\forall x \in w_1}$, $m = \sum_{\forall x \in w_2}$, $h_1^0(x,y,z) = g(x,y,z)$ and $h_2^0(x,y,z) = g_2(x,y,z)$ are the initial guesses for the estimation of back-projected functions. The advantage of this approach over standard orthogonal projection is that its equations are simpler, and they can be implemented efficiently on the computer.

3. EXPERIMENTAL RESULTS

At least two MRI data sets, acquired in orthogonal planes to each other are needed to reconstruct a high resolution isotropic volume. The reconstruction is done after registering the mutually orthogonal sequences as those seen in

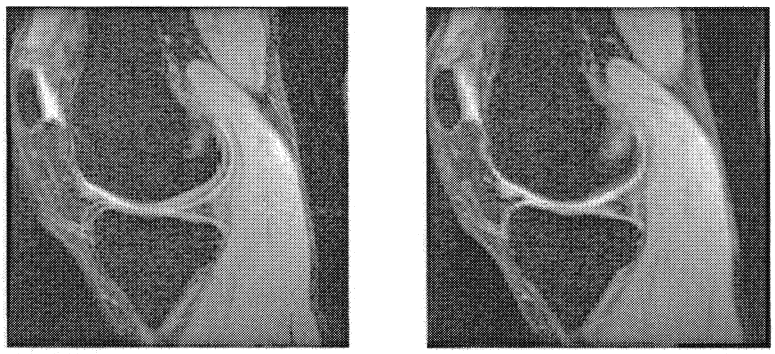

Figure 6. Left, fusion of unregistered volumes. Right, fusion after registration

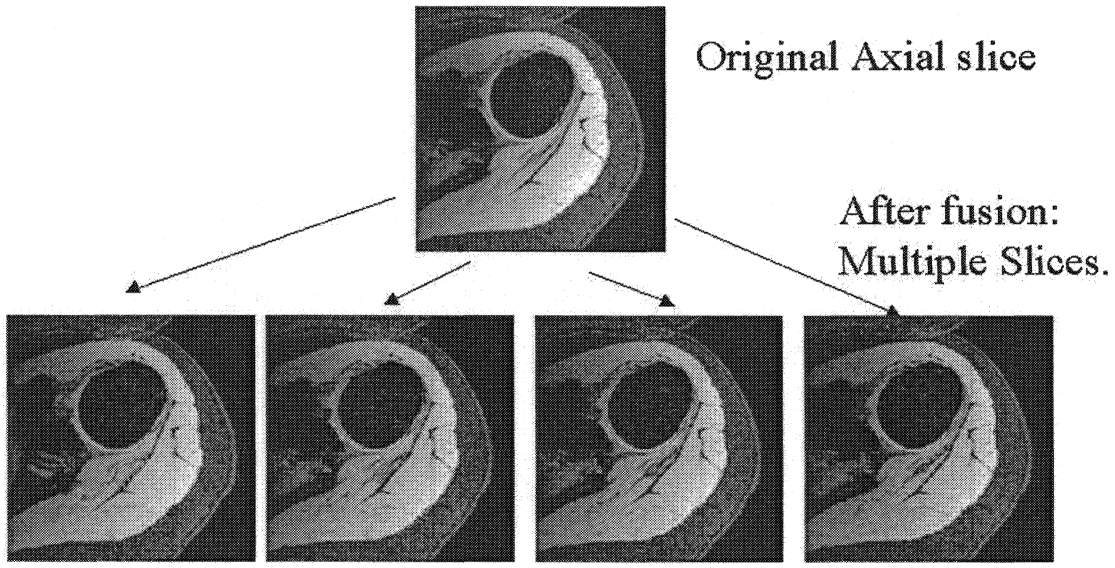

Figure 7. Shoulder fusion: One original slice and the four corresponding reconstructed slices from the fusion of two orthogonal sets.

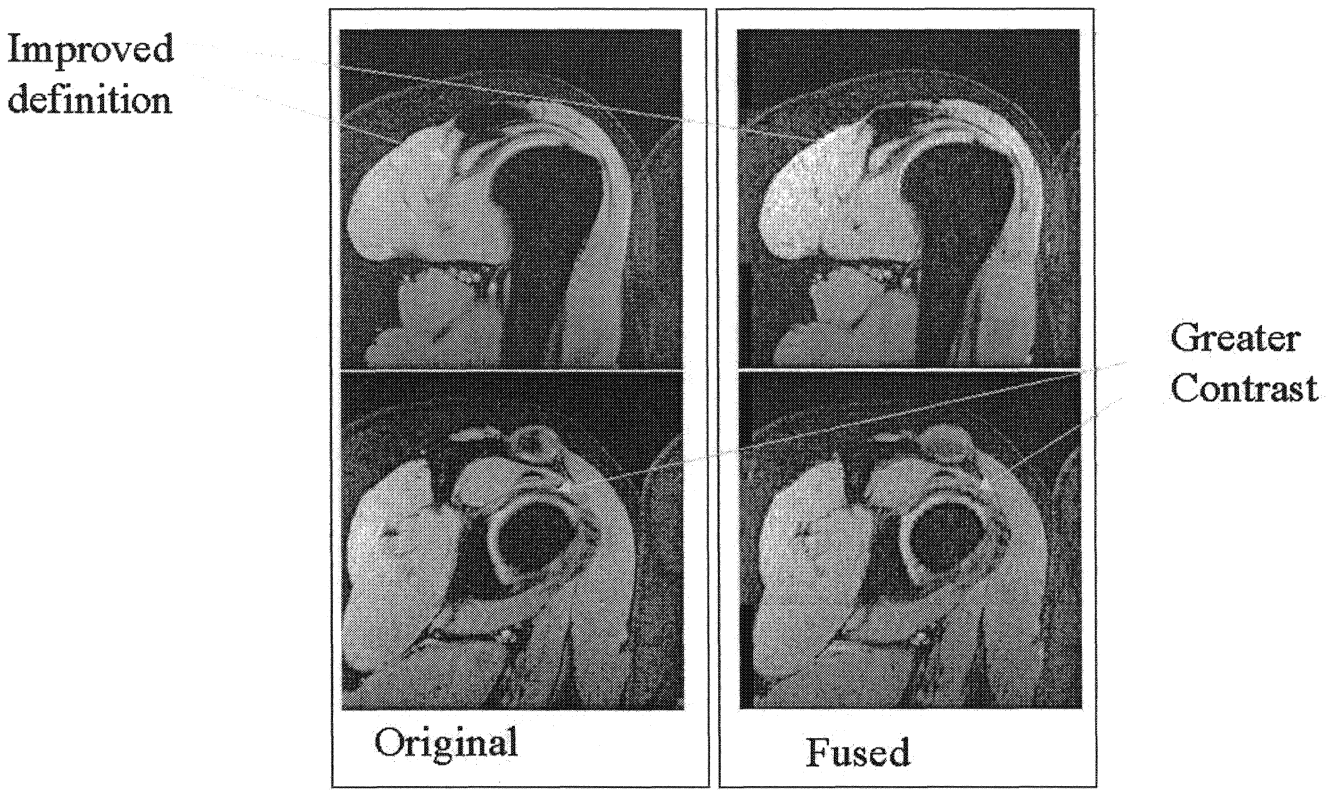

Figure 8. Improved definition and contrast of the fused shoulder image.

Figure 1. The registration is done by assuming a simple translation-rotation model and by maximizing the correlation between the magnitude of image gradient. The maximization was done using a very simple hill-climbing algorithm. Figure 6 shows the result of fusing a data set with and without registration. Once both orthogonal sets have been registered to each other, we proceed to fuse them into a single isotropic volume. A back projection model is used to reconstruct the isotropic image. This model allows the use of projection on convex sets (POCS) to solve the set of linear equations that minimize the reconstruction error from the two original MRI sets. To validate the algorithm one volunteers shoulder and four volunteers knees and one wrist were MR imaged on a 1.5 T Signa Horizon (GE, Milwaukee) clinical imager. The shoulder images were acquired in coronal and axial, the knee and the wrist in coronal and sagittal plane using 10 or 11 cm FOV, 7 cm for the wrist, 256 x 256 matrix, and 1.5 mm slice thickness except 1 mm slice thickness for the wrist and 2 mm for the shoulder. The images were acquired using a 3D GRE sequence with TE adjusted to produce T1 or T2 *-weighted information. For shoulder and knee at least one of the data sets was also fat suppressed. Image data sets were then transferred to a Silicon Graphics Octane workstation for data fusion and segmentation. To validate the registration and fusion algorithm the registered and fused data sets were reformatted to produce two orthogonal 3D imaging series to correspond to the original images. Further the fused and non-fused image data sets were reformatted to produce nonorthogonal planes. All these series as well as the original image series were evaluated in the following way. The visualization and the borders of menisci, articular cartilage, synovium, subchondral bone plates, cortex, muscle in knee and labrum, bone, subchondral bone plate, capsule, muscles in the shoulder and cartilage, subchondral bone plates and cortex in the wrist were evaluated. After that, the results were compared. To evaluate the effect of the fusion to the image segmentation both the fused data sets and the fat suppressed original data sets were segmented using our segmentation algorithm. Then the segmented 2D images and 3D image data sets were evaluated in the following way. In the knee the segmentation of both menisci, that of the articular cartilage of lateral and medial condyles in fused 2D and 3D image sets were compared to the segmentation from the original data sets. In the shoulder the segmentation of labri and cartilage was evaluated in the same way.

In the fused image sets the reformatted slices had a slice thickness which corresponded to the in-plane resolution

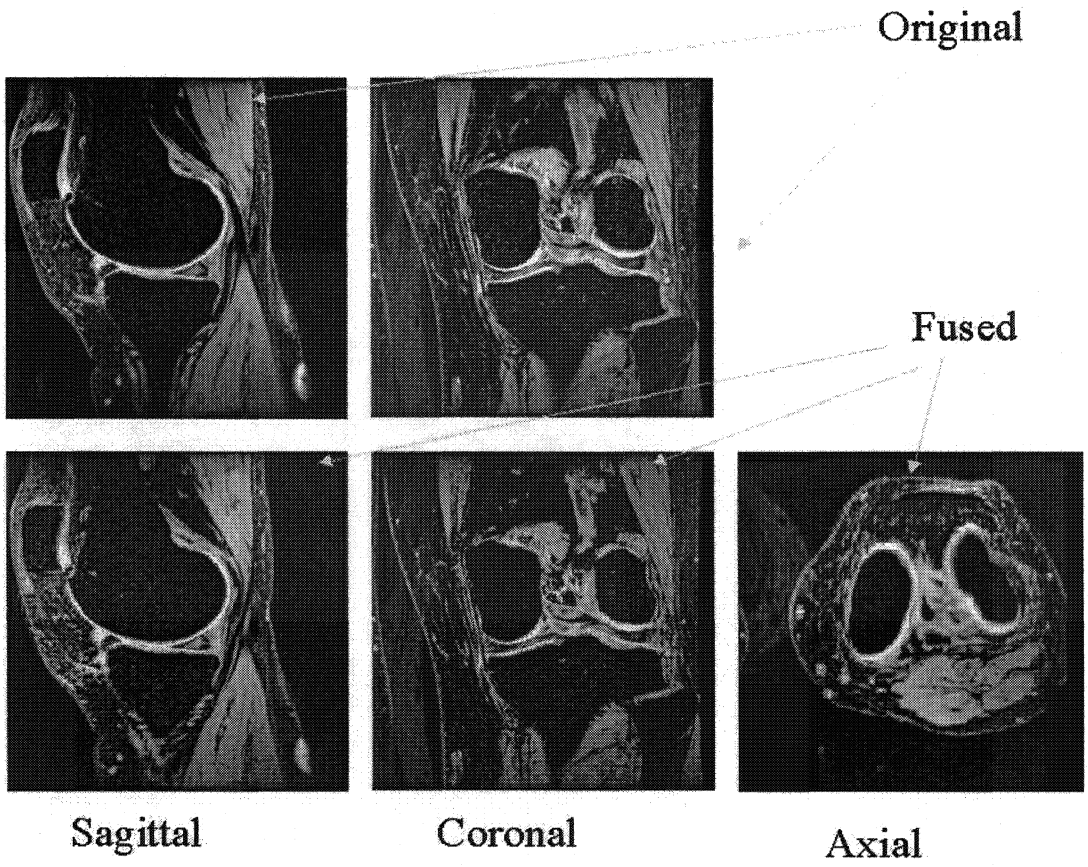

Figure 9. Improved definition and contrast: Knee fusion

of the original data sets. Therefore the number of reformatted 2D images at least tripled in the fused data sets. The increased number of slices allowed evaluation of the structures in more slices than the original data sets as seen in Figure 7. In some cases the joint had changed its position between the acquisition of two data sets6. Since the algorithm registered the second data set along the first data set the anatomic structures in the fused reformatted slices did not orient exactly in the same way as they did in the original images. Therefore, when the images were compared to each other several images from the fused data set needed to be compared to one of the original data sets. When the visualization of the borders of anatomic structures were compared to each other, the anatomic structures in the knee, shoulder and wrist fused images were better defined than in the original images. Cortical bone as well as the subchondral bone plates appeared thinner in the fused images. This difference was especially clear in the nonorthogonal images. Figure 8 and 9 show the improved definition of these features on the fused images.

4. CONCLUSION

This study showed that our registration and fusion algorithm can register and fuse orthogonal 3D GRE images even if there is slight motion between the acquired image series. It also showed that the fused data sets with ISO-resolution improved structure detection and definition. The isotropic volumes created allows high resolution evaluation of the structures in arbitrary planes. This will improve the detection of those anatomic structures whose anatomic direction does not allow their visualization in a routine orthogonal imaging plane. This study also showed that improved resolution improved the segmentation of small anatomic structures of the joints including cartilage and menisci in the knee and cartilage and labri in the shoulder. The chemical shift artifact in the fused orthogonal images however causes blurring of the images. Therefore is preferred that the fused sequences should be fat suppressed. If water only/ fat only sequence, which eliminates the chemical shift artifact, is used for image acquisition, misregistration, however, can be avoided.

ACKNOWLEDGMENTS

This work is supported in part by the NSF/NYS Grant to the Center for Electronic Imaging Systems at the University of Rochester, the University of Rochester departments of Electrical Engineering and Radiology and by a Fulbright Scholarship from the U.S.-Mexico Fulbright-CONACYT Commission, Mexico.

REFERENCES

1. G. A. Wright, "Magnetic resonance imaging," *Signal Processing* , pp. 56–66, 1997.
2. V. S, G. C, M. FB, and et al, "Improved intracranial lesion characterization by tissue segmentation based on a 3d feature map," *Magn Reson Med* **37**, pp. 457–469, 1997.
3. V. S, G. CF, K. R, and et al., "Fast tissue segmentation based on a 4d feature map in characterization of intracranial lesions," *J Magn Reson Imaging* **9**, pp. 768–776, 1999.
4. J. G. Tamez-Peña, S. Totterman, and K. J. Parker, "Unsupervised statistical segmentation of multispectral volumetric mr images," in *Proceedings SPIE, Medical Imaging 1999: Image Processing*, vol. 3661, pp. x–x, SPIE, 1999.
5. J. G. Tamez-Peña, S. Totterman, and K. J. Parker, "The integration of automatic segmentation and motion tracking for 4d reconstruction and visualization of musculoskeletal structures," in *Proceedings IEEE Workshop on Biomedical Image Analysis*, pp. 154–163, IEEE, 1998.
6. G. A.A. and T. D.A., "Fusion of short-axis and long-axis cardiac mr images," *Computarize Medical Imaging and Graphics* **20**(2), pp. 77–87, 1996.
7. J. B. A. Maintz and M. A. Viergever, "A survey of medical image registration," *Medical Image Analysis* **2**(2), pp. 1–36, 1998.
8. J. B. A. Maintz, P. A. van den Elsen, and M. A. Viergever, "Comparison of edge-based and ridge-based registration of ct and mr brain images," *Medical Image Analysis* **1**(2), pp. 151–161, 1996.
9. C. Studholme, D. L. G. Hill, and D. J. Hawkes, "Automated 3d registration of mr and ct images of the head," *Medical Image Analysis* **1**(2), pp. 163–175, 1996.
10. B. Vemuri, S. Huang, S. Sahni, M. Leonard, C. Mohr, R. Gilmore, and J. Fitzsimmons, "An efficient motion estimator with applications to medical image registration," *Medical Image Analysis* **2**(1), pp. 79–98, 1998.
11. H. Stark and Y. Yang, *Vector Space Projections*, John Wiley & Sons, INC, New York, 1998.